



Enhanced Thermoelectric Generator Power Output Based on Electrodeposited Bi₂Te₃ Nanocomposites with Pt NPs-CNTs Through Multiphysics Simulation

Muhd Aliff Ikhwan Che Azman¹, Khairul Fadzli Samat^{1,*}, Young Seng Hong¹, Jariah Mohamad Juoi¹, Rose Farahiyah Munawar¹, Hairul Effendy Ab Maulod¹, Nguyen Van Toan², Takahito Ono²

¹ Faculty of Industrial and Manufacturing Technology and Engineering, Universiti Teknikal Malaysia Melaka, 76100, Durian Tunggal, Melaka, Malaysia

² Department of Mechanical Systems Engineering, Tohoku University, Aoba-ku, Sendai 980-8579, Japan

ARTICLE INFO

Article history:

Received 29 July 2024

Received in revised form 2 September 2024

Accepted 10 October 2024

Available online 30 November 2024

Keywords:

Thermoelectric generator (TEG); CFD; nanocomposite; TEG power density

ABSTRACT

Thermoelectric generators (TEG) possess the potential to transform unused heat into electrical energy, making thermoelectricity a viable alternative for addressing the energy issue. This study provides insight into the enhanced power density of a TEG device when embedded with bismuth telluride (Bi₂Te₃) nanocomposite. The TEG power density has been analysed under the fluid flow simulation condition by utilizing several Bi₂Te₃ nanocomposite materials with Pt NPs-CNTs inclusion. The impact of static and steady air flow conditions has been studied using a detailed computational fluid dynamics (CFD) parameter, with flow velocities of 0.01 m/s and 1 m/s. As a main part of the work, the power density of nanocomposites embedded as N-type legs was compared to that of pure material. The Bi₂Te₃ with hybrid nanocomposite produces the highest power density, precisely combining Bi₂Te₃ with platinum nanoparticles (Pt Nps) and single-wall carbon nanotube (SWCNT) materials (Bi₂Te₃/Pt-SWCNTs). At velocity of 1 m/s, the power density was calculated to be 156.85 μW/cm², which increased to 158.86 μW/cm² at a fluid velocity of 1 m/s, marking an 88% increment compared to the TEG model using pristine Bi₂Te₃ and higher than that of the previous work about 4 times of increment.

1. Introduction

The demand for sustainable energy solutions has spurred intensive research into advanced technologies capable of efficiently harnessing and converting waste heat into electrical power. Among these technologies, thermoelectric generators (TEG) have garnered significant attention due to their inherent ability to convert thermal gradients directly into usable electricity [1-3]. As the global pursuit of environmentally friendly and economically viable energy sources intensifies, the purpose for enhancing the efficiency of TEG becomes increasingly paramount. TEG is a solid-state device that

* Corresponding author.

E-mail address: khairul.fadzli@utem.edu.my

<https://doi.org/10.37934/armne.25.113>

converts the thermal energy from heat flux into electrical energy using the Seebeck effect [4,5]. It offers numerous benefits, including eco-friendly energy production, extensive scalability adaptable to various heat sources, reduced production expenses, the capacity to repurpose spent heat energy, and a dependable energy supply. However, thermoelectric generators have a generally low energy conversion efficiency rate in today's technology [6,7].

In recent years, significant research efforts have been dedicated to enhancing the energy conversion efficiency of these devices, expanding their range of applications from specialized to more widespread use [8,9]. Device efficiency is generally contingent upon the performance of materials, which is intricately linked to the figure of merit. The figure of merit, denoted as ZT , is a quantitative measure defined by the equation $ZT = (S^2\sigma)/kT$, which involves the values of Seebeck coefficient (S), electrical conductivity (σ), thermal conductivity (k) and absolute temperature (T) of a thermoelectric material [10]. The thermoelectric parameters exhibit a considerable interdependence, posing a significant obstacle to their independent manipulation. Therefore, a slight increase in ZT is typically noticed, as enhancing one parameter tends to have a negative impact on others and vice versa. Bismuth telluride (Bi_2Te_3) is one of the cutting-edge thermoelectric materials utilised in commercial applications especially for low temperature applications [11]. Nevertheless, the thermoelectric performance of pure Bi_2Te_3 experiences a significant decline of approximately 86% when formed through the electrochemical deposition process [12]. Electrochemical deposition is preferred in the synthesis process due to its cost-effectiveness and ease of integration into batch production processes [13]. In response to the low thermoelectric performance, numerous studies related to the nanocomposite's initiative have been conducted and successfully contributed to the improvement [14-16].

In this work, the structural TEG model has been comprehensively developed to replicate a fabricated TEG module. The module, which has been fabricated and contains a deposit of Bi_2Te_3 -based material, is used for a comparative analysis. The incorporation of nanocomposites to Bi_2Te_3 has been verified to enhance the Seebeck coefficient. Nevertheless, there is uncertainty regarding its efficacy in enhancing power density and temperature difference during fluid flow simulation condition. This study involves a Multiphysics simulation and evaluates power density estimations of the TEG device using several nanocomposite materials. The main variables that are being altered in this study are the Bi_2Te_3 -based nanocomposite utilised in TEG devices and the heat transfer parameter in the simulation setup. Prior to conducting the simulation, the model of the TEG device was developed based on a fabricated device [17]. The TEG model consists of 28 pairs of thermoelectric modules and encompassed an interconnect layer with silicon (Si) cover for both surfaces of TEG. This study measures the nanocomposite power density in the simulated TEG device. This work improves the power density efficiency of a thermoelectric generator (TEG) module and the temperature differential at various fluid velocities.

2. Model Development

2.1 Numerical Model

Recently, numerical models have become extensively utilized to calculate the precise results of TE devices using commercial software such as ANSYS or COMSOL Multiphysics [18,19]. Convective heat transfer can be modelled using computational fluid dynamics (CFD) tools and analytical models that rely on empirical formulations. Most research has focused on simulating the thermal-electric multi-physics of a single thermoelectric (TE) couple or module and the fluid-thermal multi-physics of a TE generator system [20,21]. However, when the TE generator system is utilized to recover waste heat from fluids, it is essential to include the fluid-thermal multi-physical coupling effects and the

thermoelectric effects. Relying solely on results generated from CFD modelling may result in a lack of accuracy [22-24]. The TE generator system involves fluid-thermal-electric multi-physical fields, which encompass several parameters such as, convective heat transfer, Fourier heat conduction, and thermoelectric properties. The air dissipates in the flow channel of the heat exchanger and heat sink, following the concepts of mass, momentum, and energy conservation as following Eqs. (1) to (3).

$$\nabla \cdot v = 0 \quad (1)$$

$$\nabla \cdot (vv) = \frac{1}{\rho} \nabla p + \nabla \cdot (\mu \nabla v) \quad (2)$$

$$\nabla \cdot (\kappa \nabla T) = \rho c v \cdot \nabla T \quad (3)$$

where v is the fluid velocity; ρ is the fluid density; p is the fluid pressure; μ is the dynamic viscosity; κ is the thermal conductivity, and c is the specific heat. Besides, the renormalization group (RNG) k - ε turbulence model is adopted in this work, which has a higher adaptivity and accuracy than other turbulence models. The specifications of Eq. (4) and Eq. (5) provided have been used to represent the fluid zones [21]. Its transportation equations are:

$$\frac{\partial}{\partial t} (\rho \kappa) + \frac{\partial}{\partial x_i} (\rho \kappa u_i) = \frac{\partial}{\partial x_j} \left(\alpha_k \mu_{eff} \frac{\partial \kappa}{\partial x_j} \right) + G_k + G_h - \rho \varepsilon - Y_M \quad (4)$$

$$\frac{\partial}{\partial t} (\rho e) + \frac{\partial}{\partial x_i} (\rho \varepsilon u_i) = \frac{\partial}{\partial x_j} \left(\alpha_k \mu_{eff} \frac{\partial \varepsilon}{\partial x_j} \right) + G_{1\varepsilon} \frac{\varepsilon}{k} (G_k + G_{3\varepsilon} G_b) - C_{2\varepsilon} \rho \frac{\varepsilon^2}{k} - R_\varepsilon \quad (5)$$

Eq. (6) and Eq. (7) encompass the Fourier and the Joule heats correlation. The last component on the right-hand side of the equation represents either the Peltier heat at the junctions or the Thomson heat along the P-type and N-type TE materials. The steady-state energy conservation correlation in P-type and N-type semiconductors serve as fundamental power sources as follows:

$$\nabla \cdot (\kappa_p(T) \nabla T_p) = -\sigma_p^{-1}(T) J^2 + \nabla \alpha_p(T) J T_p \quad (6)$$

$$\nabla \cdot (\kappa_n(T) \nabla T_n) = -\sigma_n^{-1}(T) J^2 + \nabla \alpha_n(T) J T_n \quad (7)$$

where $\sigma_{p,n}^{-1}(T)$ and $\alpha_{p,n}(T)$ represents the electrical conductivity, and Seebeck coefficient of the P-type and N-type thermoelectric materials, respectively. J is the current density vector. Nevertheless, the energy conservation equations for copper electrodes and ceramic plates differ from those of semiconductors because copper lacks the Seebeck effect, and ceramics lack both the Seebeck effect and the Joule effect. These equations can be represented by Eq. (8) for copper and Eq. (9) for ceramics:

$$\nabla \cdot (\kappa_{co} \nabla T) = -\sigma_{co}^{-1} J^2 \quad (8)$$

$$\nabla \cdot (\kappa_{ce} \nabla T) = 0 \quad (9)$$

where κ_{co} and σ_{co}^{-1} are the thermal conductivity and electrical resistivity of copper material, and κ_{ce} is the thermal conductivity of ceramic material.

2.2 TEG Model Development and Meshing Quality

This work employs the integrated N-type nanocomposite within the simulated TEG device. Prior to conducting simulation work on the nanocomposite TEG device, the TEG model and the simulation setup has been validated with the experiment of TEG fabricated device. This is done to prevent any potential inaccuracies in the simulation due to erroneous parameters. The TEG model was developed by replicating the exact geometrical dimensions of the fabricated device [25,26]. Both the N-type and P-type materials used are doped with nickel in bismuth telluride ($\text{Ni-Bi}_2\text{Te}_3$) and with antimony telluride (Sb_2Te_3), respectively. Figure 1 depicts the comparison between the TEG device that was created and the simulation model.

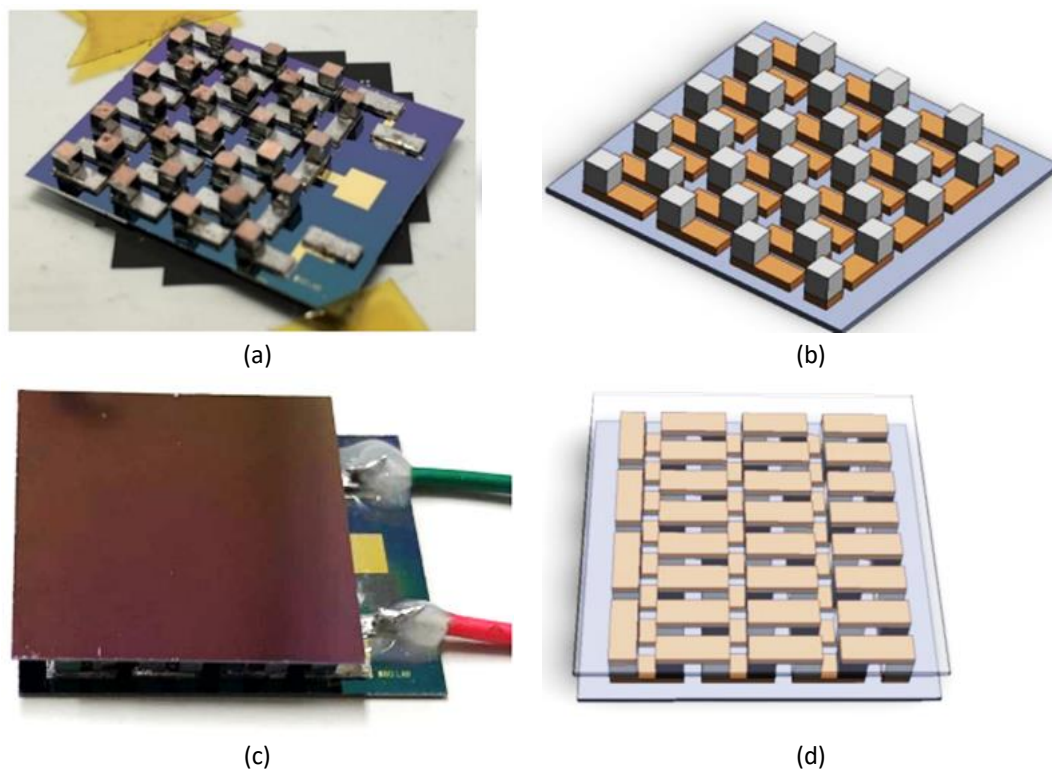


Fig. 1. Device comparison between the fabricated TEG device and the simulation model (a) Fabrication process on the N-type material installation (b) Development process in the simulation model with exact geometrical dimension as the fabricated device (c) Completed TEG device (d) Full model of TEG device

Meshing is a crucial step that must be precisely planned in fluid dynamics simulation. The number of elements created in the meshing process should be considered to get better and more accurate results for a complex geometrical model. However, a high number of elements requires a longer calculation time. Therefore, an appropriate number of elements should be considered during the meshing process. To achieve a good quality of mesh, certain criteria should be followed. The criteria are aspect ratio around value of 1, Jacobian value around 1, skewness value in between 0-0.5 and most important, minimum orthogonal quality having a value of 0.1 [27-29]. Orthogonal quality is a measure of alignment between normal vectors of the cell faces and vectors connecting cell centroids with face centroids and with centroids of neighbouring cells. The concept of orthogonal quality in meshing is relating to how close the angles between adjacent element faces (or adjacent element edges) are to some optimal angles [30]. The TEG model has achieved a good quality mesh

requirement by having the minimum orthogonal quality value of 0.20, aspect ratio value of 1.86, Jacobian ratio of 1.0 and skewness value of 0.23 as shown in Table 1.

Table 1

Element-node and meshing quality parameter	
Element-node/mesh metric	Parameter
Node	2 589 724
Element	13 051 676
Minimum orthogonal quality	0.2001
Average aspect ratio	1.8636
Average Jacobian ratio	1
Skewers	0.2330

2.3 Material and Thermoelectric Properties

The simulation model has been created by referencing the crucial elements of the manufactured TEG device. The Si substrates were coated with a substance covering the top and bottom sides of the TEG. Additionally, Cu was used as an interconnecting layer between the thermolegs (N-type and P-type materials). Figure 2 illustrates the presence of nanocomposite materials in the TEG [8]. Due to their fragile condition, the simulation model does not include the SiO₂ (500 nm) and Cr/Au (220 nm) layers in the constructed device [25]. The cumulative thickness of the disregarded components was less than 0.5% compared to that of the Si substrate. It was presumed that these thin layers were unaffected by the temperature variation. Table 2 and Table 3 display the essential material properties and thermoelectric properties required for the simulation, including density, heat capacity, and thermal conductivity. For Table 3, Ni/Bi₂Te₃ was used for comparison analysis with author's previous work of fabricated TEG.

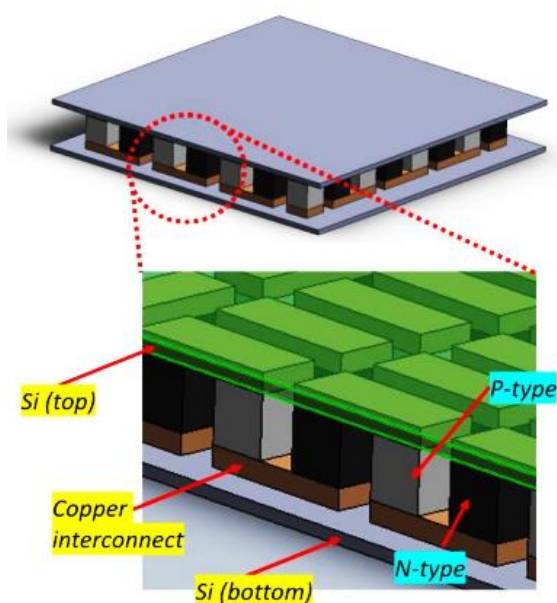


Fig. 2. The material used in the TEG model is commonly known as a manufactured device

Table 2

Material properties of Cu (interconnecting layer), Si (substrate) and Al (heat sink)

Material properties	Cu [31]	Al	Si
Density, (kg/m ³)	8900	2719	2328
Heat capacity, (J/kgK)	385	871	710
Thermal conductivity, (WmK)	400	202.4	0.2

Table 3

N-type and P-type materials properties for conducting the simulation

Material properties	P-type:	N-type					
	Sb ₂ Te ₃ [32,33]	Ni/Bi ₂ Te ₃ [32]	Bi ₂ Te ₃ [32,33]	Pt (1.9wt%)/ Bi ₂ Te ₃ [16]	Pt SWCNTs/Bi ₂ Te ₃ [34]	MWCNT (3.5wt%) / Bi ₂ Te ₃ [34]	SWCNTs (3.8wt%) / Bi ₂ Te ₃ [34]
Density (Kg/m³)	6440	7670	7670	7670	7670	7670	7670
Heat capacity (J/KgK)	214	198	198	198	198	198	198
Thermal conductivity (WmK)	1.30	0.70	1.55	0.87	0.49	0.47	0.47
Seebeck coefficient ($\mu\text{V/K}$)	170	-140	-115	-184	-226	-61	-51
Resistivity, $\frac{1}{\sigma} - n(\Omega\text{cm})$ $\times 10^{-3}$	2.50	1.03	1.62	1.89	3.44	0.98	0.67

2.4 Boundary Condition

The fluid entrance was positioned at the front of the 3D model, while the fluid outflow was placed at the back of the 3D model. Furthermore, the lower section of the TEG model remains exposed due to the absence of coverage from the surrounding box [33,35]. The simulation involved positioning the lower portion of the TEG model on top of a heat source. Subsequently, the environment was arranged to mimic the conditions of a room, including maintaining room temperature. Table 4 illustrates the fluid input, fluid outflow, and the lower section of the TEG model. Once the boundary condition of the 3D model and its surroundings have been established, the subsequent step is to define the parameters for the simulation setup. The simulation was configured to replicate real-life conditions, with the lower section of the TEG model positioned directly over a heat source.

Table 4

Fluid flow and temperature parameter

Simulation parameter	
Inlet fluid velocity (m/s)	0.01 and 1
Surrounding temperature	24°C
Applied temperature on the bottom part of TEG	30°C

In addition, the simulation was configured to simulate airflow within the TEG device and heatsink. In this simulation, two distinct fluid velocity values are utilized. One is set at 0.01m/s to replicate a scenario with minimal airflow. However, a velocity of 1m/s is used to imitate the movement of an investigator carrying the device and walking at a regular walking speed. Table 5 presents the heat transfer coefficient parameter used in the simulations. Meanwhile, Figure 3 displays the complete configuration of the TEG simulation, including the heat sink.

Table 5
 Forced convection heat transfer coefficient of different materials

Materials	Heat transfer coefficient for fluid velocity 0.01m/s, (W/m ² K)	Heat transfer coefficient for fluid velocity 1m/s, (W/m ² K)
Aluminum	8.0	23.0
Copper	10.0	25.0
Silicon	95.0	95.0
Bismuth telluride	15.7	15.7
Antimony telluride	30.0	40.0

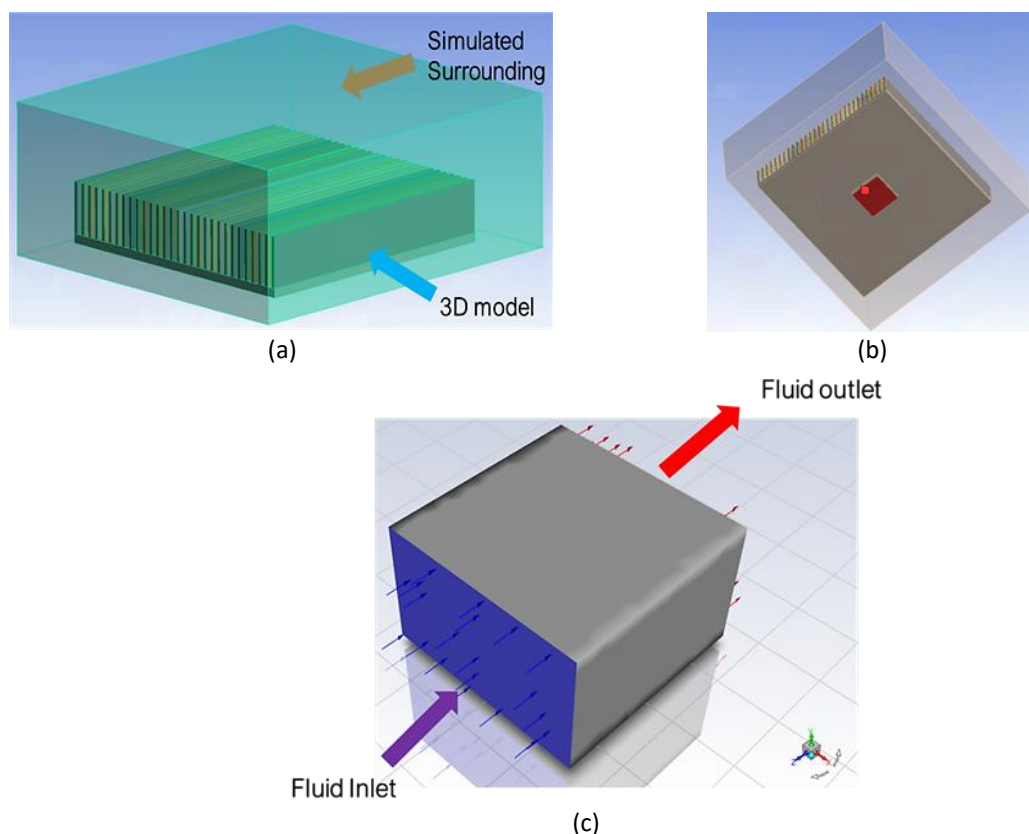


Fig. 3. Simulation setup (a) The whole 3D model (TEG with heat sink) (b) Bottom part of the TEG with heat sink models (c) Fluid flow inlet-outlet

2.5 Maximum Electrical Power Analysis

The electrical power produced by a TEG device is determined by the architectural design, the temperature differential, and the thermoelectric qualities. The TEG device incorporates many thermocouples to amplify the total output of Seebeck voltage. The maximum power output (P_{max}) can be calculated by considering the number of thermocouples (n) as following Eq. (10).

$$P_{max} = n(S_P - S_N)^2 \Delta T^2 / 4R \quad (10)$$

where $S_{P,N}$ Seebeck voltage for N-type or P-type material, and R is the total electrical resistance materials. The electrical resistance of the materials can be expressed as Eq. (11).

$$R = \rho_P h_P A_P^{-1} + \rho_N h_N A_N^{-1} \quad (11)$$

where h is high or thickness of thermocouples, $\rho_{P,N}$ is electrical resistivity and $A_{P,N}$ is cross section of thermocouples. In TEG device, the cross section and the thickness of thermocouple should be equal. Therefore, the maximum power generated at designated thickness, $P_{h,max}$ can be expressed as following Eq. (12) [36].

$$P_{h\ max} = \frac{nA\Delta T^2}{h} \left[\frac{(S_P - S_N)^2}{4(\rho_P + \rho_N)} \right] \quad (12)$$

The expression is neglecting the electrical and thermal contact resistances, and it can be expected that the calculated value will be much higher than the actual application.

3. Results

3.1 Temperature Difference on Meshing Quality

The temperature difference in this study is measured by obtaining both the lowest (the side that connected with the heat sink) and the highest temperatures of the thermolegs as shown in Figure 4. Table 6 displays the temperature differences observed between pure material and nanocomposite placed on N-type films. These differences were measured for all components of the 3D model, taking into consideration the forced convection heat transfer coefficient.

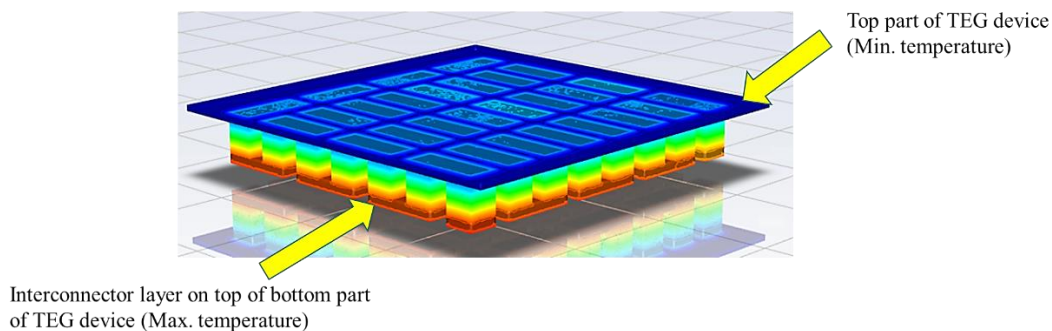


Fig. 4. TEG module in fluent simulation

Table 6

Utilising a low mesh quality and appropriate mesh quality to measure the temperature differential in a material

	Low mesh		Appropriate mesh	
	Ni/Bi ₂ Te ₃	Bi ₂ Te ₃	Ni/Bi ₂ Te ₃	Bi ₂ Te ₃
Max. temperature (°C)	28.9221	28.8437	29.2021	29.0017
Min. temperature (°C)	24.0815	24.0914	24.24	24.2749
Temperature difference, °C	4.8406	4.7523	4.9621	4.7268
Temperature difference between different materials (°C)	-0.09		-0.20	

The low mesh quality indicates that the temperature difference between the pure material and the material embedded with nanocomposite is only marginally different, with a discrepancy of approximately 0.09. The meshing quality needs to be improved, resulting in accurate and imprecise generated outcomes. An inaccurate result will result in an incorrect computation of the output power generated by the investigated TEG device. In addition, the accurate mesh analysis reveals a substantial temperature difference of approximately 0.21 between the pure material and the material implanted with nanocomposite. A notable disparity becomes evident upon comparing this

outcome with the previously observed subpar meshing quality. Given that the meshing quality meets the criterion for good meshing quality, this meshing configuration possesses a good meshing quality.

3.2 Validation of Power Density with Experimental Results

As indicated in Table 7, the difference in power density value between the author's previous experimental work [32] and this simulation result was very noticeable. The aim is to compare the power density of a TEG made of Ni/Bi₂Te₃ material with that of Bi₂Te₃, which has inferior thermoelectric characteristics. Various variables contribute to the discrepancy between the power density simulation value and the experimental value, one of which is the presence of contact resistance in the experimental setup. The presence of imperfections in the contacts between different materials can lead to increased resistance, hence decreasing the effectiveness of the TEG. While simulations typically assume perfect contact, real application conditions often entail some level of contact resistance, particularly at interfaces.

In addition, heat loss to the surroundings, which may not be accurately considered in the simulation, can decrease the temperature difference across the thermoelectric materials, reducing the power generated by the TEG [32]. Considering factors such as conduction, convection, and radiation losses is important. Finally, even slight discrepancies in material qualities between the simulation and actual conditions can result in variances in performance. These parameters encompass properties such as thermal conductivity, electrical conductivity, Seebeck coefficient, and carrier mobility. Even slight variations in these characteristics can affect the overall effectiveness of the TEG.

Table 7

Comparing power density between experimental and simulated results

	Experimental [32]		Simulation	
	Bi ₂ Te ₃	Ni/Bi ₂ Te ₃	Bi ₂ Te ₃	Ni/Bi ₂ Te ₃
Power density (μW/cm ²)	15	111	116	176

3.3 Power Density and Temperature Difference

Table 8 depicts the power density and temperature differential of various nanocomposite materials incorporated into an N-type film at fluid velocities of 0.01m/s and 1m/s. Generally, as the flow rate rises, the temperature difference for all the TEGs, even in different nanocomposite integrations, increases. The fluid flow increases the heat transfer rate, particularly on the heat sink, resulting in a lower temperature on the TEG's cold side. The power density generated for the pristine Bi₂Te₃ reaches 101.87 μW/cm² at 1 m/s of flow rate, with the lowest temperature differential as compared to nanocomposites. The results are consistent with previous findings, where the power density range that can be obtained from the TEG model with the pure Bi₂Te₃ at N-type material was 87.5-137.5 μW/cm² [36,37]. MWCNTs/Bi₂Te₃ and SWCNTs/Bi₂Te₃ nanocomposites contribute the highest temperature changes due to a lower thermal conductivity as compared to pristine Bi₂Te₃. The films exhibit the same temperature difference in both circumstances due to their identical thermal conductivity.

The power density increases significantly when the Bi₂Te₃ has been improved with Pt nanoparticles inclusion as shown in Figure 5. It reaches 156.85 μW/cm² and 158.86 μW/cm² of power density at 0.01m/s and 0.1m/s fluid velocities, respectively. The results of the simulation are significantly affected by the specified thermoelectric material properties. In the author's previous work, the Pt-SWCNTs/Bi₂Te₃ nanocomposite achieved a remarkable thermoelectric figure of merit,

ZT, of 0.99, an increase of approximately 68% compared to pure Bi₂Te₃. The nanoinclusion of Pt nanoparticles and single-walled carbon nanotubes (SWCNTs) altered the electron density and formed a large phonon scattering, which improved the Seebeck coefficient and thermal conductivity, respectively. The bismuth telluride nanocomposite, composed of SWCNTs and multi-walled carbon nanotubes (MWCNTs), exhibits the most significant disparity in temperature due to its reduced thermal conductivity [34]. In addition, the lower Seebeck coefficient for both films results in even lower power density output for TEG.

Table 8

Power density ($\mu\text{W}/\text{cm}^2$) and temperature difference ($^{\circ}\text{C}$) on fluent simulation at flow velocities of 0.01 m/s and 1 m/s

N-type materials / fluid velocity	Power density ($\mu\text{W}/\text{cm}^2$)		Temperature difference ($^{\circ}\text{C}$)	
	0.01 m/s	1 m/s	0.01m/s	1m/s
Bi ₂ Te ₃	100.10	101.87	4.39	4.43
MWCNTs/Bi ₂ Te ₃	92.14	93.29	4.78	4.81
SWCNTs/Bi ₂ Te ₃	91.84	92.99	4.78	4.81
Pt/Bi ₂ Te ₃	151.71	153.78	4.50	4.53
Pt-SWCNTs/Bi ₂ Te ₃	156.85	158.86	4.76	4.79

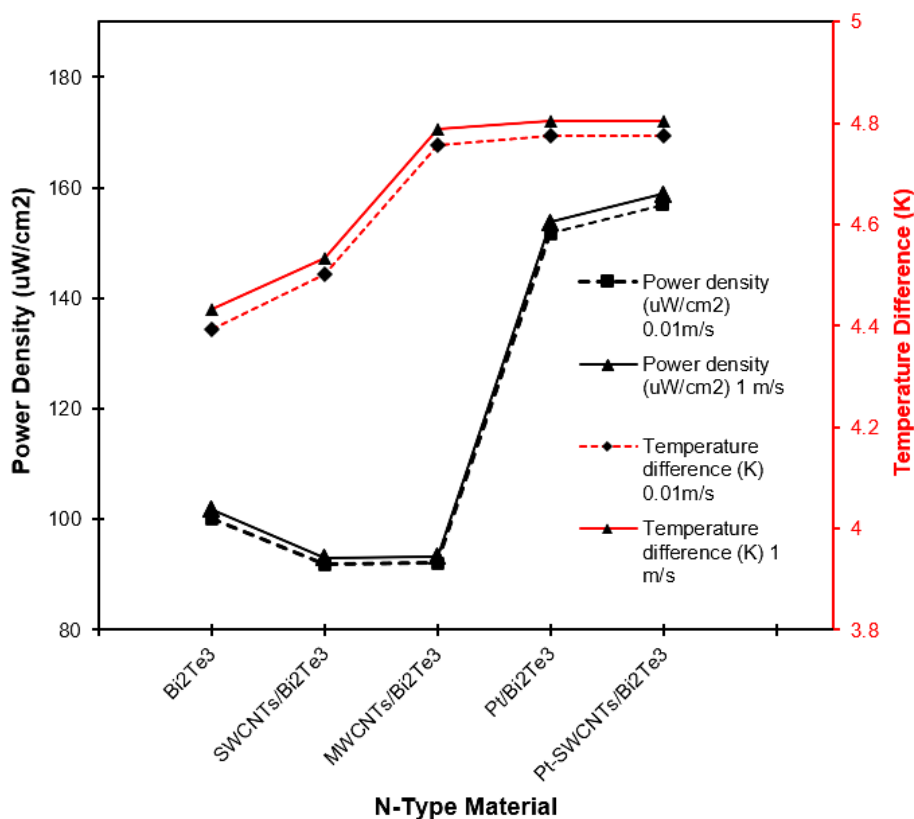


Fig. 5. Power density with different N-type nanocomposite and temperature difference generated by fluid velocity of 0.01m/s and 1m/s

4. Conclusions

In conclusion, the TEG model using the Pt-SWCNTs/Bi₂Te₃ nanocomposite exhibited the highest power density as compared to the pristine Bi₂Te₃ and other nanocomposites of CNTs and Pt nanoparticles. At a fluid velocity of 0.01 m/s, the power density was determined to be 156.85 $\mu\text{W}/\text{cm}^2$. This climbed to 158.86 $\mu\text{W}/\text{cm}^2$ at a fluid velocity of 1 m/s, representing an 88% increase

compared to the TEG model utilising pure Bi₂Te₃. Furthermore, the improvement surpassed previous finding by a factor of 4. The newly developed nanocomposite films in this study exhibited a much-improved ZT value, resulting in a substantial increase in power density as predicted by the π -type TEG model. These findings provide a more reliable method for improving μ TEG devices, especially in low-temperature environments.

In addition, the TEG structure underwent analysis through CFD simulation, yielding crucial insights into the thermal and fluid dynamics performance of the device. The validation results have substantiated the precision of the CFD model, demonstrating outstanding concurrence with experimental data. Moreover, the calibre of the mesh employed in the simulation significantly impacted the precision of the power density measurements. Utilising a high-quality meshing technique guarantees more accurate fluid flow predictions, therefore improving the reliability of the simulation results. The significance of thorough simulation and validation methodologies in optimising TEG performance is emphasised by these coupled aspects.

Acknowledgment

The study is funded by Ministry of Higher Education (MOHE) of Malaysia through the Fundamental Research Grant Scheme (FRGS), No: FRGS/1/2023/TK08/UTeM/02/5. The authors would like to thank Universiti Teknikal Malaysia Melaka (UTeM) for all the support.

References

- [1] Nozariasbmarz, Amin, Jerzy S. Krasinski, and Daryoosh Vashae. "N-type bismuth telluride nanocomposite materials optimization for thermoelectric generators in wearable applications." *Materials* 12, no. 9 (2019): 1529. <https://doi.org/10.3390/ma12091529>
- [2] Angeline, Appadurai Anitha, Jayaraj Jayakumar, and Lazarus Godson Asirvatham. "Performance analysis of (Bi₂Te₃-PbTe) hybrid thermoelectric generator." *International Journal of Power Electronics and Drives Systems* 8, no. 2 (2017). <https://doi.org/10.11591/ijpeds.v8i2.pp917-925>
- [3] Sunil, Arjun Kozhikkatil, and Rakesh Kumar. "Designing a more effective finned automotive radiator cooling process using carbon nanotube-water nanofluid turbulent flow." *Suranaree Journal of Science & Technology* 28, no. 4 (2021).
- [4] Gould, Chris, and Noel Shammis. "Three dimensional TCAD simulation of a thermoelectric module suitable for use in a thermoelectric energy harvesting system." *Small-Scale Energy Harvest* 29 (2012). <https://doi.org/10.5772/51404>
- [5] Kong, Deyue, Wei Zhu, Zhanpeng Guo, and Yuan Deng. "High-performance flexible Bi₂Te₃ films based wearable thermoelectric generator for energy harvesting." *Energy* 175 (2019): 292-299. <https://doi.org/10.1016/j.energy.2019.03.060>
- [6] Aswal, Dinesh K., Ranita Basu, and Ajay Singh. "Key issues in development of thermoelectric power generators: High figure-of-merit materials and their highly conducting interfaces with metallic interconnects." *Energy conversion and management* 114 (2016): 50-67. <https://doi.org/10.1016/j.enconman.2016.01.065>
- [7] Luo, Ding, Ruochen Wang, and Wei Yu. "Comparison and parametric study of two theoretical modeling approaches based on an air-to-water thermoelectric generator system." *Journal of Power Sources* 439 (2019): 227069. <https://doi.org/10.1016/j.jpowsour.2019.227069>
- [8] Khalif, Abdul Jabbar N., and I. R. A. A. Mousawi. "Comparison of heat transfer coefficients in free and forced convection using circular annular finned tubes." *International Journal of Application or Innovation in Engineering & Management* 5, no. 4 (2016): 194-204.
- [9] Chen, Si, Nikolaos Logothetis, Lilei Ye, and Johan Liu. "A high performance Ag alloyed nano-scale n-type Bi₂Te₃ based thermoelectric material." *Materials Today: Proceedings* 2, no. 2 (2015): 610-619. <https://doi.org/10.1016/j.matpr.2015.05.083>
- [10] Kumar, Sunil, Deepti Chaudhary, Punit Kumar Dhawan, R. R. Yadav, and Neeraj Khare. "Bi₂Te₃-MWCNT nanocomposite: an efficient thermoelectric material." *Ceramics International* 43, no. 17 (2017): 14976-14982. <https://doi.org/10.1016/j.ceramint.2017.08.017>
- [11] Ahmad, Kaleem, C. Wan, M. A. Al-Eshaikh, and A. N. Kadachi. "Enhanced thermoelectric performance of Bi₂Te₃ based graphene nanocomposites." *Applied Surface Science* 474 (2019): 2-8. <https://doi.org/10.1016/j.apsusc.2018.10.163>

- [12] Agarwal, Khushboo, Deepak Varandani, and B. R. Mehta. "Simultaneous improvement in electron transport and phonon scattering properties in Bi₂Te₃: Si nanocomposite thin films: Role of a conducting secondary phase." *Journal of Alloys and Compounds* 698 (2017): 1058-1065. <https://doi.org/10.1016/j.jallcom.2016.12.309>
- [13] Kulbashinskii, V. A., V. G. Kytin, N. V. Maslov, P. Singha, Subarna Das, A. K. Deb, and A. Banerjee. "Thermoelectrical properties of Bi₂Te₃ nanocomposites." *Materials Today: Proceedings* 8 (2019): 573-581. <https://doi.org/10.1016/j.matpr.2019.02.056>
- [14] Tang, Gui, Kefeng Cai, Jiaolin Cui, Junlin Yin, and Shirley Shen. "Preparation and thermoelectric properties of MoS₂/Bi₂Te₃ nanocomposites." *Ceramics International* 42, no. 16 (2016): 17972-17977. <https://doi.org/10.1016/j.ceramint.2016.07.083>
- [15] Nguyen, Trung Huu, Jirath Enju, and Takahito Ono. "Enhancement of thermoelectric properties of bismuth telluride composite with gold nano-particles inclusions using electrochemical co-deposition." *Journal of the electrochemical society* 166, no. 12 (2019): D508. <https://doi.org/10.1149/2.1011912jes>
- [16] Samat, Khairul Fadzli, Nguyen Huu Trung, and Takahito Ono. "Enhancement in thermoelectric performance of electrochemically deposited platinum-bismuth telluride nanocomposite." *Electrochimica Acta* 312 (2019): 62-71. <https://doi.org/10.1016/j.electacta.2019.04.139>
- [17] Hu, Xiaokai, Priyanka Jood, Michihiro Ohta, Masaru Kunii, Kazuo Nagase, Hirotaka Nishiate, Mercuri G. Kanatzidis, and Atsushi Yamamoto. "Power generation from nanostructured PbTe-based thermoelectrics: comprehensive development from materials to modules." *Energy & Environmental Science* 9, no. 2 (2016): 517-529. <https://doi.org/10.1039/C5EE02979A>
- [18] Chen, Wei-Hsin, Po-Hua Wu, and Yu-Li Lin. "Performance optimization of thermoelectric generators designed by multi-objective genetic algorithm." *Applied Energy* 209 (2018): 211-223. <https://doi.org/10.1016/j.apenergy.2017.10.094>
- [19] Wang, Yiping, Shuai Li, Xu Xie, Yadong Deng, Xun Liu, and Chuqi Su. "Performance evaluation of an automotive thermoelectric generator with inserted fins or dimpled-surface hot heat exchanger." *Applied Energy* 218 (2018): 391-401. <https://doi.org/10.1016/j.apenergy.2018.02.176>
- [20] Selimefendigil, Fatih, and Hakan F. Öztöp. "Thermoelectric generation in bifurcating channels and efficient modeling by using hybrid CFD and artificial neural networks." *Renewable Energy* 172 (2021): 582-598. <https://doi.org/10.1016/j.renene.2021.03.046>
- [21] Ebling, Dirk, Martin Jaegle, Markus Bartel, Alexandre Jacquot, and Harald Böttner. "Multiphysics simulation of thermoelectric systems for comparison with experimental device performance." *Journal of electronic materials* 38 (2009): 1456-1461. <https://doi.org/10.1007/s11664-009-0825-0>
- [22] Lan, Song, Zhijia Yang, Rui Chen, and Richard Stobart. "A dynamic model for thermoelectric generator applied to vehicle waste heat recovery." *Applied Energy* 210 (2018): 327-338. <https://doi.org/10.1016/j.apenergy.2017.11.004>
- [23] Li, Wenkai, Jiangying Peng, Wanli Xiao, Honghao Wang, Jinsong Zeng, Jin Xie, Qibai Huang, Kuanmin Mao, and Li Zhang. "The temperature distribution and electrical performance of fluid heat exchanger-based thermoelectric generator." *Applied Thermal Engineering* 118 (2017): 742-747. <https://doi.org/10.1016/j.applthermaleng.2017.03.022>
- [24] Liao, Mingjian, Zhu He, Chengpeng Jiang, Yawei Li, and Fengsheng Qi. "A three-dimensional model for thermoelectric generator and the influence of Peltier effect on the performance and heat transfer." *Applied Thermal Engineering* 133 (2018): 493-500. <https://doi.org/10.1016/j.applthermaleng.2018.01.080>
- [25] Kwan, Trevor Hocksun, and Xiaofeng Wu. "The Lock-On Mechanism MPPT algorithm as applied to the hybrid photovoltaic cell and thermoelectric generator system." *Applied energy* 204 (2017): 873-886. <https://doi.org/10.1016/j.apenergy.2017.03.036>
- [26] Zareei, Javad, Seyyed Hissein Hoseyni, and Marischa Elveny. "Study of the effect of the boundary layer excitation in the nanofluids flow inside the tube on increasing the heat transfer coefficient." *Journal of Computational & Applied Research in Mechanical Engineering (JCARME)* 12, no. 1 (2022): 109-119. <https://doi.org/10.22061/jcarme.2021.6252.1795>
- [27] Fatchurrohman, N., and S. T. Chia. "Performance of hybrid nano-micro reinforced mg metal matrix composites brake calliper: simulation approach." In *IOP conference series: materials science and engineering*, vol. 257, no. 1, p. 012060. IOP Publishing, 2017. <https://doi.org/10.1088/1757-899X/257/1/012060>
- [28] Duan, Jiabin, Jiawei Zhao, Xinke Li, Satyam Panchal, Jinliang Yuan, Roydon Fraser, and Michael Fowler. "Modeling and analysis of heat dissipation for liquid cooling lithium-ion batteries." *Energies* 14, no. 14 (2021): 4187. <https://doi.org/10.3390/en14144187>
- [29] Parlak, Zekeriya, Yaşar İslamoğlu, and Nezaket Parlak. "Performance evaluation of an integrated heatsink and thermoelectric module by two-way coupled numerical analysis." *International Journal of Thermal Sciences* 197 (2024): 108809. <https://doi.org/10.1016/j.ijthermalsci.2023.108809>

- [30] Hameed, Majid M., Muhamad Bin Mansor, Mohd Azrin Mohd Azau, and Ahmed Kadhim Alshara. "Computational design and analysis of LiFePO₄ battery thermal management system (BTMS) using thermoelectric cooling/thermoelectric generator (TEC–TEG) in electric vehicles (EVs)." *Journal of Energy Storage* 72 (2023): 108394. <https://doi.org/10.1016/j.est.2023.108394>
- [31] Jayabalan, Jaya, Murali Govindarajan, Vajhala Venu Madhav, and Kannammal Jayabalan Sabareesaan. "Thermal management for green vehicle batteries under natural and forced convection modes." *Current Applied Science and Technology* (2022): 10-55003. <https://doi.org/10.55003/cast.2022.04.22.002>
- [32] Van Toan, Nguyen, Truong Thi Kim Tuoi, Khairul Fadzli Samat, Hongtao Sui, Naoki Inomata, Masaya Toda, and Takahito Ono. "High performance micro-thermoelectric generator based on metal doped electrochemical deposition." In *2020 IEEE 33rd International Conference on Micro Electro Mechanical Systems (MEMS)*, pp. 570-573. IEEE, 2020. <https://doi.org/10.1109/MEMS46641.2020.9056358>
- [33] Xue-Dong, Liu, and Yong-Ho Park. "Structure and transport properties of (Bi_{1-x}Sb_x)₂Te₃ thermoelectric materials prepared by mechanical alloying and pulse discharge sintering." *Materials Transactions* 43, no. 4 (2002): 681-687. <https://doi.org/10.2320/matertrans.43.681>
- [34] Samat, Khairul Fadzli, Yijie Li, Nguyen Van Toan, Mohd Asyadi Azam, and Takahito Ono. "Highly enhanced thermoelectric and mechanical properties of Bi₂Te₃ hybrid nanocomposite with inclusion of Pt nanoparticles and SWCNTs." *Journal of Materials Research* 37, no. 20 (2022): 3445-3458. <https://doi.org/10.1557/s43578-022-00694-z>
- [35] Nazer, Mohamed, Muhammad Fadzrul Hafidz Rostam, Se Yong Eh Noum, Mohammad Taghi Hajibeigy, Kamyar Shameli, and Ali Tahaei. "Performance analysis of photovoltaic passive heat storage system with microencapsulated paraffin wax for thermoelectric generation." *Journal of Research in Nanoscience and Nanotechnology* 1, no. 1 (2021): 75-90. <https://doi.org/10.37934/jrnn.1.1.7590>
- [36] Gould, Chris, and Noel Shammass. "Three dimensional TCAD simulation of a thermoelectric module suitable for use in a thermoelectric energy harvesting system." *Small-Scale Energy Harvest* 29 (2012). <https://doi.org/10.5772/51404>
- [37] Mostafavi, Seyed Alireza, and Mojtaba Mahmoudi. "Modeling and fabricating a prototype of a thermoelectric generator system of heat energy recovery from hot exhaust gases and evaluating the effects of important system parameters." *Applied Thermal Engineering* 132 (2018): 624-636. <https://doi.org/10.1016/j.applthermaleng.2018.01.018>